JACS
JOURNAL OF THE AMERICAN CHEMICAL SOCIETY
pubs.acs.org/JACS
Communication

$MnBi_2$ Is a Permanent Magnet

Catherine K. Badding,[▽] Eric A. Riesel,[▽] Ryan A. Murphy, Danilo Puggioni, Dmitry Popov, Gilberto Fabbris, Daniel Haskel, James M. Rondinelli,* Alison B. Altman,* and Danna E. Freedman*

Cite This: J. Am. Chem. Soc. 2025, 147, 25129−25135
Read Online
ACCESS | Metrics & More | Article Recommendations | Supporting Information

ABSTRACT: Creating and understanding new permanent magnets requires an understanding of the impact of orbital angular momentum on coercivity. A simple approach to interrogating this relationship is by incorporating high Z (where Z is the atomic number) elements into binary compounds to maximize spin−orbit coupling. The Mn−Bi system is an appealing platform for these studies since it contains MnBi, a permanent magnet with a large coercive field. We previously identified a new compound in the Mn−Bi system, $MnBi_2$, but could not elucidate its magnetic properties ex situ due to its decomposition upon decompression. Here, we harnessed synchrotron X-ray magnetic circular dichroism to probe the magnetism of $MnBi_2$ at high pressure within a diamond anvil cell. Our results indicate that $MnBi_2$ exhibits ferromagnetic hysteresis at both 10 K and room temperature. Through calculations and experiments, we show that orbital angular momentum and spin−orbit coupling from Bi impart magnetic anisotropy in $MnBi_2$. Comparing the Mn−Bi family of compounds, we consider the Bi p and d orbitals to explain the differences in magnetic behavior within the system. Collectively, these results validate leveraging high-Z elements in the synthesis of new hard permanent magnets.

Permanent magnets are foundational to our society—they are at the core of technologies ranging from energy generators to data storage.[1−3] Tuning magnetic properties to gain insight into the core variable of coercivity or resistance to demagnetization is crucial for the design of the next generation of magnetic technologies. A critical determinant of a material's coercivity is its magnetocrystalline anisotropy, an intrinsic measure of the energy required to reorient the magnetization. This magnetocrystalline anisotropy arises from spin−orbit coupling (SOC), but the impact of SOC depends on several variables, including structure, orbital hybridization, energy overlap, and band structure, limiting our ability to harness large SOC intentionally. To better understand the interplay between these factors and SOC, we sought out a simple binary system, where one atom bears spin (e.g., manganese), and the other bolsters orbital angular momentum retained via strong SOC (e.g., bismuth). This approach mimics the magnetic design principles of lanthanide-based permanent magnets by coupling the spin and orbital moments across two separate atoms, offering a route toward rational alternatives to rare-earth-based materials.

The Mn−Bi system is an attractive testbed for examining the impact that structural modification has on SOC, as even small changes in crystal structure and stoichiometry can have outsized impacts on magnetic properties. For example, MnBi is a hard permanent magnet that exhibits unusual coercivity trends, where, contrary to typical ferromagnets, the coercive field increases with the temperature. Modulating the crystallographic a/c ratio induces a spin reorientation transition (SRT) that is normally observed only at low temperature.[4−18] After undergoing the SRT, MnBi is a soft ferromagnet with negligible coercivity. In contrast, the high-temperature $Mn_{1.05}Bi$ phase, a modified version of the MnBi phase where the Mn atoms move into the interstitial sites of MnBi, is a canted soft magnet with sluggish spin dynamics.[9] We previously harnessed high pressure to add an additional phase to the Mn−Bi system, $MnBi_2$, by compressing to 8.3 GPa and heating above at least 400 K. We expect $MnBi_2$ to exhibit ferromagnetic order similar to its ambient pressure congener.[19] This expectation is supported by prior density functional theory (DFT) calculations which predicted that $MnBi_2$ is a ferromagnet, exhibiting spontaneous spin polarization and magnetocrystalline anisotropy energy (MAE) of comparable magnitude to MnBi.[19,20] Yet, in contrast to the subtle crystallographic differences between MnBi and $Mn_{1.05}Bi$, $MnBi_2$ is structurally distinct, and subsequently, we expect the coercivity, saturation magnetization, and temperature dependence of the ferromagnetic behavior to change dramatically, offering a powerful opportunity for comparison.

Given that $MnBi_2$ does not persist at ambient pressure, magnetic characterization necessitates high-pressure measurements beyond the capabilities of conventional SQUID magnetometry. The conventional diamond anvil cells (DACs) we use to synthesize $MnBi_2$ and maintain the phase at high pressure contribute a background signal that greatly exceeds that from a relatively negligible sample quantity. In this context, in-situ high-pressure magnetometry techniques, such as AC susceptibility, neutron diffraction, magnetic field sensing via endogenous nitrogen-vacancy pair defects in a DAC, and X-

Received: April 23, 2025
Revised: July 3, 2025
Accepted: July 3, 2025
Published: July 15, 2025

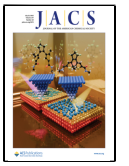

https://doi.org/10.1021/jacs.5c06874
J. Am. Chem. Soc. 2025, 147, 25129−25135

ray circular dichroism spectroscopy (XMCD), provide routes for understanding the impact of pressure on magnetic materials.[21−31]

XMCD spectroscopy is particularly well-suited for in-situ magnetic characterization of samples at high pressure.[17,24,25,32−35,32−35,35−42] This technique measures the magnetic polarization of a system by examining the differential absorption of left- and right-circularly polarized X-rays.[43,44] By tuning the X-ray energy to match a specific core-level electronic transition, XMCD selectively measures the response of a specific element, providing insight into how individual elements contribute to the overall magnetic behavior of a material.[45−48] XMCD is highly sensitive to subtle changes in the magnitude and orientation of the orbital and spin moments that may occur with variable temperature and pressure conditions.[17,35,42] In our case, these capabilities allow us to directly probe the contribution from Bi atoms to the magnetism of $MnBi_2$ without a spurious signal from potential magnetic impurities. Herein, we report the experimental observation of room-temperature ferromagnetism in $MnBi_2$ at a high pressure. Comparative XMCD analysis and calculations of compounds in the Mn−Bi system allow us to rationalize differences in their coercivity through the factors which impact the expression of SOC, offering a path for the next generation of ultrahard permanent magnets.

To access homogeneous samples of $MnBi_2$ appropriate for magnetic characterization, we used a full-cell resistive heating approach adapted from previously reported synthetic conditions.[19] Briefly, we heated MnBi and Bi to 648 K at 7 GPa in a nonmagnetic cell, and used powder X-ray diffraction (PXRD) to monitor the growth of peaks corresponding to $MnBi_2$. We considered the reaction complete when diffraction peaks belonging to MnBi were no longer observable (Figure 1).[32]

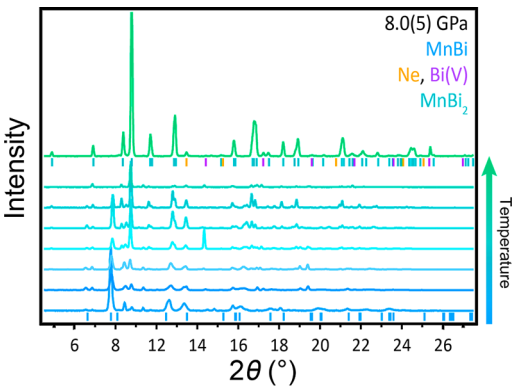

Figure 1. Background-subtracted X-ray diffraction patterns (λ = 0.413280 Å) showing the conversion of the precursor sample to $MnBi_2$. Bi(V) refers to the highest-pressure polymorph of bismuth.

Isolating pure MnBi precursor is challenging as this material is not a congruently melting phase; instead, it involves a peritectic reaction between Mn and a Mn−Bi melt. Thus, our precursor was a mixture of MnBi and its elemental constituents. We did not observe Mn peaks in the PXRD of our precursor, although amorphous Mn was likely present, as the precursor powder contained a stoichiometric 1:1 ratio of Mn and Bi, as determined by energy-dispersive X-ray spectroscopy (Figure S2). We observed diffraction from Bi prior to heating, and the disappearance of the diffraction peaks belonging to Bi suggests that the reaction proceeds via a peritectoid mechanism, i.e., the incorporation of Bi into MnBi to form $MnBi_2$. We do not observe the presence of elemental Mn via diffraction, although we should note that amorphous Mn cannot be excluded. While this could indirectly impact the results, Mn alone would not induce the ferromagnetism we observe.

To interrogate the magnetic properties of $MnBi_2$, we focused on Bi since chemical intuition regarding SOC, calculations, and prior work all support bismuth having a large role in dictating the magnetic behavior of MnBi.[12,13,49] Specifically, we performed X-ray absorption spectroscopy (XAS) and XMCD experiments on Bi $L_{3,2}$-edges (13.419 and 15.711 keV, respectively) at Beamline 4-ID-D at the Advanced Photon Source at Argonne National Laboratory. In these XMCD experiments, we used circularly polarized light to probe the spin polarization of Bi 6*d* electronic states directly. Measuring the difference in the population of available Bi 6*d* "spin-up" and "spin-down" holes affords a net spin polarization value.[48] Note that the small amount of Bi observed via PXRD should not contribute significantly to the XMCD signal. We expect the high-pressure bismuth polymorph, Bi(V), to remain a diamagnet at high pressure, similar to the ambient pressure polymorph, Bi(I). In the case where Bi(V) becomes a paramagnet instead, we would still expect that Bi(V) would not exhibit ferromagnetic signatures such as remanence or coercivity. In $MnBi_2$, however, we expect the hybridization of Mn 3*d*, Bi 6*d*, and 6*p* states to result in a small ferromagnetic net moment on Bi. Indeed, our calculations suggest that the Bi sites should have moments of 0.003 and 0.005 μB (Table 1).

Table 1. Calculated Magnetic Moments and Magnetocrystalline Anisotropy Energy of $MnBi_2$ at 8.4 GPa and MnBi at 0 GPa

	$MnBi_2$	MnBi
magnetic moment on Bi 6*d* states (μB)	0.003, 0.005	0.011
total magnetic moment (μB)	6.256	6.965
magnetocrystalline anisotropy energy (MJ/m^3)	0.205	0.275

While small, these moments residing on Bi sites proved sufficient to detect an XMCD response, thus providing us with a spectroscopic handle to measure the magnetic properties of $MnBi_2$. Finally, by relying on a technique that probes the atomic core states of Bi, we ensure that we are probing the magnetic behavior of $MnBi_2$, rather than nominal magnetic impurities such as elemental Mn. While Mn 3*d* states account for most of the magnetic moment in $MnBi_2$, measuring the XMCD at the Mn K-edge (6.54 keV) at high pressures poses significant challenges due to a combination of an inherently small XMCD signal (~0.1% of the absorption jump), and strong X-ray absorption by both the heavy Bi ions and diamond anvils.

Our XMCD measurements demonstrate that the Bi 6*d* bands of $MnBi_2$ are broadened over a wide energy range and do not exhibit a clear white line, complicating standard quantifications of individual m_s *and* m_l components with the use of sum rules (Figure 2).[30] We instead calculated the ratio of orbital and spin contributions to the magnetic moment, m_l/m_s, which we derive using the $L_{3,2}$ XMCD areas ($\Delta A_{3,2}$) by integrating from 13.41 keV to 13.45 keV for L_3 and from 15.71 keV to 15.75 keV for L_2. While this analysis would ideally involve integrating the entire L_3 and L_2 range to satisfy XMCD sum rules, such an analysis is challenging for states spread over

https://doi.org/10.1021/jacs.5c06874
J. Am. Chem. Soc. 2025, 147, 25129−25135

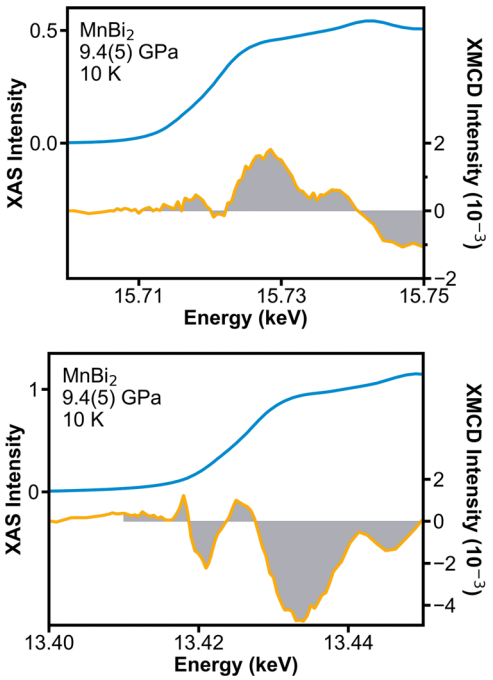

Figure 2. Experimental Bi XAS (blue) and XMCD (orange) response of $MnBi_2$ at 9.4(5) GPa, 10 K, and ∓2 T at the L_2 edge (left). The shaded regions indicate integrated regions. Experimental Bi XAS (blue) and XMCD (orange) response of $MnBi_2$ at 9.4(5) GPa, 10 K, and ∓2 T at the L_3 edge (right). The shaded regions indicate that the regions were integrated. The principles of XMCD are described in detail in ref 48.

large energy ranges. Assuming a negligible magnetic dipole operator, as is common in the analysis of powder-averaged samples, we approximate the ratio of m_l/m_s as[17,50,51]

$$\frac{m_l}{m_s} = \frac{2(\Delta A_3 + \Delta A_2)}{3(\Delta A_3 - 2\Delta A_2)}$$

At 9.4(5) GPa, 10 K, and ∓ 2 T, we find that $\Delta A_3 = -4.82 \times 10^{-5}$ (arb. units) and $\Delta A_2 = 1.04 \times 10^{-5}$ (arb. units). In $MnBi_2$, the m_l/m_s ratio (0.37) is positive, indicating that the Bi 6*d* spin and orbital moments align parallel. Compared to the m_l/m_s ratio measured for MnBi (0.05) at 300 K, $MnBi_2$ (0.37) has an order of magnitude larger m_l/m_s ratio at 10 K.[17] Multiplying the experimental fractions of orbital moment versus total moment, 0.05 and 0.27, by the calculated total magnetic moment on Bi 6*d* states, 0.011 and 0.003 μB, the resulting product indicates the orbital moment on the Bi 6*d* states are 0.0005 and 0.0008 μB for MnBi and $MnBi_2$, respectively. We assign the relatively large orbital moment of Bi 6*d* states in $MnBi_2$ to the additional spin−orbit coupling imparted by a higher composition of Bi which we expect to result in a large magnetic anisotropy, consistent with analysis performed on related systems.[17,52−55]

The hallmark of permanent magnetism is hysteretic behavior, where the material retains magnetization without an applied magnetic field. Thus, to probe whether $MnBi_2$ is a permanent magnet, we undertook field-dependent XMCD measurements at 10 K and 9.4(5) GPa. First, we magnetically polarized $MnBi_2$ at 6 T, and then recorded the XMCD signal while sweeping the field from 6 T to −6 T. Upon changing the field from 6 T to 0 T, we observed nearly constant intensities of the XMCD signal within the uncertainty of our measurement, indicating significant remnant magnetization (Figure 3). Polarizing the sample in the opposite direction to −1 T, we observe that the XMCD signal switches sign, and eventually saturates at −2 T. Next, sweeping the field from −6 T to 6 T, we likewise see full inversion of the XMCD signal at 2 T. We performed two different methods to estimating the coercive field from the hysteresis curve. First, we used a linear interpolation between 0 and 1 T on the background-subtracted data, which symmetrizes the hysteretic curve (Figure S10). We obtained the *x*-intercepts of ±0.61 T. However, due to the coarse 1 T sampling interval and the high likelihood that the magnetization curve is nonlinear near the coercive region, this is not a precise measurement of coercive field. Our second estimation involved fitting one branch of the hysteresis curve with an arctangent model (see the Supporting Information for details). In doing so, we estimate the coercive field to be −0.631 ± 0.195, which is in agreement with the estimation from linear interpolation. We emphasize that this is a rough indicator of the width. Based on this interpolation and the remnant moment being significantly nonzero, we estimate the coercive field to lie in the range of 0.436 T to 0.826 T, suggesting that $MnBi_2$ is a hard magnet.

Having established that $MnBi_2$ is a hard ferromagnet at low temperatures, we next investigated the temperature-dependent magnetic properties of $MnBi_2$ by performing abbreviated hysteresis loops up to room temperature. The remanent magnetization decreases as the temperature increases from 10 K to 300 K, but remains nonzero, indicating $MnBi_2$ retains

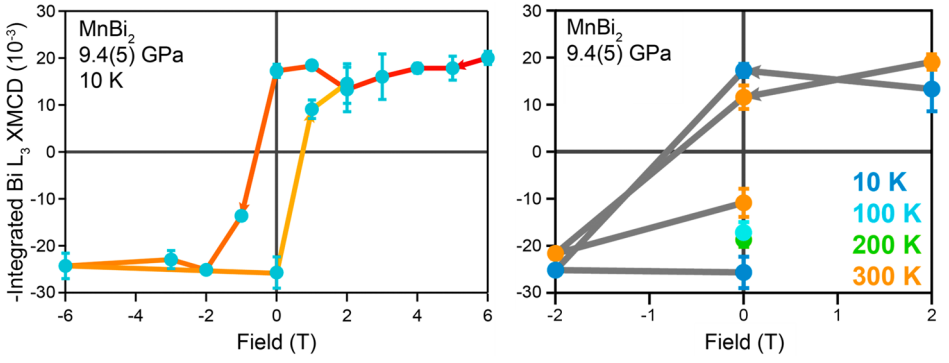

Figure 3. Integrated XMCD signal vs magnetic field plot of $MnBi_2$, showing hysteresis at 9.4(5) GPa and 10 K (left); XMCD signal vs magnetic field plot of $MnBi_2$ as a function of temperature, showing hysteresis at 300 K (right). Error bars indicate the standard deviation of the XMCD signal across several XMCD scans at each temperature, field, and pressure condition.

https://doi.org/10.1021/jacs.5c06874
J. Am. Chem. Soc. 2025, 147, 25129−25135

ferromagnetism at room temperature. Meanwhile, the magnetic saturation moment does not significantly change with temperature, as demonstrated by the abbreviated hysteresis loop performed at 300 K. Taken together, these data suggest a Curie temperature of over 300 K in $MnBi_2$.

Comparing MnBi, $Mn_{1.05}Bi$, and $MnBi_2$, we note distinct differences in magnetic behavior. MnBi undergoes a spin reorientation transition (SRT) at 90 K, and, unusually, the coercive field increases as temperature increases.[4−18] Previous literature suggests this to be related to the magnetic structure evolving from an "easy-cone" magnetic texture along the *ab*-plane at low temperatures to a collinear, easy-axis magnetic structure along the *c*-axis at high temperatures. $Mn_{1.05}Bi$, meanwhile, contains Kagome lattice layers and is a soft ferromagnet, exhibiting negligible coercivity and a noncollinear, dynamic magnetic structure.[9] In both cases, the spin−orbit interaction is a critical component of these complex and evolving magnetic structures. In contrast, our results on $MnBi_2$ suggest that the temperature dependence of its magnetic structure is less complex and does not exhibit evidence of a SRT, as the coercivity and remanence are comparatively less perturbed by temperature changes.

To better understand these results, we consider the factors contributing to the coercivities of MnBi and $MnBi_2$. We measured the coercivity of a MnBi polycrystalline sample prepared similarly to the one used for the synthesis of $MnBi_2$ at ambient pressure using vibrating sample magnetometry (VSM), resulting in values of 0.045 T at 300 K and 0.005 T at 10 K (Figure S22). These coercivities are significantly lower than the values reported in the literature, which reach 1 T (via XMCD) at 300 K and 2.5 T (using VSM) at 540 K. Despite its low coercivity, our sample has similar magnetization values at 5 T (55 emu/g) to those reported in the VSM experiment (60 emu/g) at room temperature.[10,17] In a prior XMCD experiment, Yang and co-workers[10] have reported on arc-melting, grinding, heating, and cryomilling to synthesize polycrystalline MnBi, and in a different experiment using VSM, Choi and co-workers[17] have reported on arc-melting an ingot and creating ribbons out of the ingot, which they annealed before grinding, to create nanocrystalline MnBi. Our synthesis involved ball-milling and heating without any arc-melting, a simplified procedure, as we did not optimize our synthesis for improved coercivity by microstructure engineering. We expected that the high-pressure transformation of the sample from MnBi to $MnBi_2$ could result in a different microstructure in $MnBi_2$ compared to the precursor. Regardless, these results highlight that converting our MnBi sample to $MnBi_2$ significantly improved the coercivity, despite the $MnBi_2$ sample consisting of strained, unoriented polycrystals. We expect that, with more experimentation on the synthetic conditions of $MnBi_2$, we may enhance the coercivity of the $MnBi_2$ sample even further, given that we report the estimated coercive field on a sample without any attempts to optimize the microstructure. The upper bound for the coercivity for $MnBi_2$ is likely less than MnBi, since the calculations show that the MAE of $MnBi_2$ is smaller than that of MnBi.

Our results showed that m_l/m_s is an order of magnitude larger for $MnBi_2$ than MnBi. In practice, the experimental m_l/m_s ratio of a sample has a limited dependence on the microstructure as well. As previously discussed, the reported m_l/m_s ratio for MnBi was measured on a more pristine sample than on our highly strained $MnBi_2$ sample. This suggests that the m_l/m_s ratio of $MnBi_2$ could be even greater than that of MnBi in a sample with an engineered microstructure. This might lead us to expect larger magnetic anisotropy in $MnBi_2$ compared to MnBi. However, the *total* magnetic moment residing on the Bi atoms (0.003 and 0.005 μB) is several times smaller in $MnBi_2$ than that in MnBi (0.011 μB) based on our calculations. Experiments show that the Bi spin and orbital moments are of the same sign, negating any considerations that the spin and orbital moments may both be large but cancel each other out.

The smaller Bi moment is due to a broader 6*d* band in $MnBi_2$, and our calculations demonstrate this via fewer Bi 6*d* states in $MnBi_2$ (0.013 and 0.0058 states/eV/f.u. for up and down states, Figure S18) than literature values for MnBi (0.018 and 0.047 states/eV/f.u. for up and down states) at the Fermi level.[56] We posit that the difference in the magnitude of the moment on Bi may explain, at least in part, the smaller coercivity in $MnBi_2$ compared to ideal MnBi samples: while the Bi moments in $MnBi_2$ are more anisotropic, the Bi 6*d* contribution to the magnetic behavior in $MnBi_2$ is significantly smaller compared to MnBi.[10,17] We note that $MnBi_2$ coercivity could still be maximized via microstructure engineering. Additionally, while the tabulated Bi 6*d* orbital moment is higher in $MnBi_2$ than in MnBi, magnetic coupling strongly influences the effect of the Bi orbital moment on magnetocrystalline anisotropy. As the magnetic moment and unfilled states on Bi 6*d* orbitals stems from interactions with neighboring Mn and Bi atoms, we expect that stronger coupling leads to a larger moment on the Bi 6*d* orbitals. Thus, we conclude that the smaller moment on the Bi 6*d* states suggests the coupling is weaker between the Bi 6*d* states and Mn 3*d* states. Our calculations support this explanation, as the MAE of $MnBi_2$ is only 75% of that found in MnBi (Table 1).

We expect the remaining contribution to coercivity to come from the Mn orbitals, as is demonstrated in MnBi, where the orbital moment of Mn significantly contributes, even more so than the Bi orbital moment.[49,56,57] The difference in the Mn crystal field geometries between MnBi and $MnBi_2$ largely dictates the role of Mn in the MAE of $MnBi_2$ (Figure 4). Specifically, the trigonal antiprism coordination environment of MnBi leads to a degree of unquenched orbital angular momentum, whereas the square antiprism coordination in $MnBi_2$ quenches the orbital angular momentum by breaking the degeneracy of *d* states.[58]

A key parameter for developing new permanent magnets is the MAE. We performed calculations that indicate that $MnBi_2$ has a significant magnetic moment (6.256 μB) and magnetocrystalline anisotropy energy (0.205 MJ/m^3) (Table 1). This compares favorably to elemental magnetism in Fe, Co, and Ni (magnetic moments of 2.2, 1.7, and 0.6 μB, respectively, and MAE of 0.017, 0.85, and 0.042 MJ/m^3, respectively).[59,60] In comparison, industrial permanent magnets relying on lanthanide elements, such as $Nd_2Fe_{14}B$ and $SmCo_5$, have higher magnetic moments (38.1 and 9.4 μB, respectively) and greater MAE (4.9 and 24.3 MJ/m^3, respectively).[59,61−63] This contextualizes the performance of $MnBi_2$, compared with industry standards.

We suspect that MnBi exhibits a SRT while $MnBi_2$ lacks one, due to the difference in the bonding nature of the Bi *p*-orbitals. In MnBi, the SRT is driven by anisotropic Bi−Bi *p*-orbital pair exchange striction, which is connected to temperature-based changes in the *a*/*c* crystallographic ratio.[49] We suspected that the *p*-orbital contribution to the magnetic moment was smaller

https://doi.org/10.1021/jacs.5c06874
J. Am. Chem. Soc. 2025, 147, 25129−25135

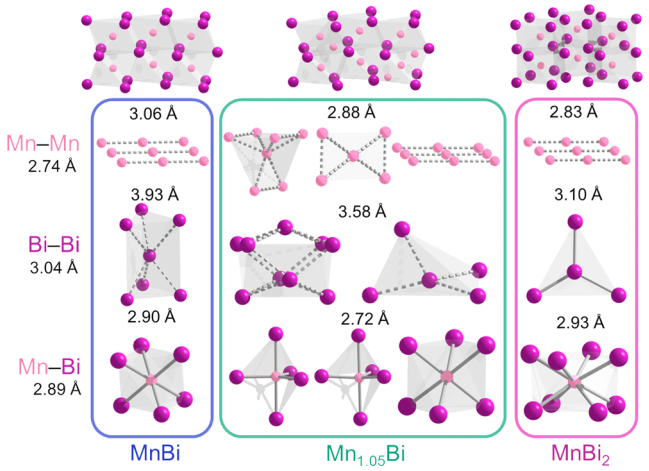

Figure 4. Representations of Mn and Bi coordination environments in MnBi (left)[8] and $Mn_{1.05}Bi$ (middle)[6] at ambient pressure and $MnBi_2$[7] at 8.7 GPa with the shortest bond distance indicated above. We note below the labels the shortest bonds within elemental Mn and Bi at ambient pressure. Multiple octahedral environments in $Mn_{1.05}Bi$ do exist. Pink and purple spheres represent Mn and Bi atoms, respectively.

in $MnBi_2$ compared to MnBi, which, in turn, would lead to less striction, preventing an SRT from occurring. However, we calculated that Bi 6*p*-orbitals in $MnBi_2$ have a magnetic moment of −0.088 and −0.096 μB, while the literature reports that MnBi Bi 6*p*-orbitals have a magnetic moment of −0.09 μB, suggesting that the magnitude of *p*-orbital magnetic moments does not lead to the difference in magnetic behavior (Table S8).[56] This is consistent with the comparable bonding distances between the Mn and Bi atoms in MnBi and $MnBi_2$. However, examining the Bi subsystem, the Bi atoms in MnBi are clearly nonbonding, while bonding in $MnBi_2$. We suggest that a significant contributing factor to the lack of SRT in $MnBi_2$ is that the stronger bonding between the Bi atoms reduces the localization of the Bi *p*-orbitals, reducing the anisotropy of the orbitals that is crucial to the SRT.

Our findings demonstrate that $MnBi_2$ is a permanent ferromagnet with an estimated coercive field within the range of 0.436−0.826 T at 10 K and retains its ferromagnetic properties up to room temperature. Compared to MnBi, which has unusual temperature-dependent magnetic behavior, our XMCD results suggest that $MnBi_2$ is more akin to conventional magnetic phases. We argue that this significant orbital moment shows SOC contributions from Bi impart magnetic anisotropy in $MnBi_2$, although the weaker coupling between the Bi 6*d* and Mn 3*d* states fails to maximize the coercive field compared to MnBi. The delocalized Bi *p*-orbitals are also likely responsible for the lack of a deleterious SRT in $MnBi_2$, affording superior coercivity at low temperatures. Our analysis of the Mn−Bi system supports the rational design of novel permanent magnets using high-Z elements with sizable SOC to contribute orbital magnetic moments and impart magnetocrystalline anisotropy. More generally, these results illustrate the value of in-situ high-pressure measurements in unveiling magnetic behavior and demonstrating the differences in properties among congeners within the same system.

■ ASSOCIATED CONTENT

Supporting Information

The Supporting Information is available free of charge at https://pubs.acs.org/doi/10.1021/jacs.5c06874.

Synthesis and characterization details, experimental methods, computational methods, tables and figures of data (PDF)

■ AUTHOR INFORMATION

Corresponding Authors

James M. Rondinelli − *Department of Materials Science and Engineering, Northwestern University, Evanston, Illinois 60208, United States;* orcid.org/0000-0003-0508-2175; Email: jrondinelli@northwestern.edu

Alison B. Altman − *Department of Chemistry, Texas A&M University, College Station, Texas 77843, United States;* orcid.org/0000-0002-4975-5004; Email: aaltman@tamu.edu

Danna E. Freedman − *Department of Chemistry, Massachusetts Institute of Technology, Cambridge, Massachusetts 02139, United States;* orcid.org/0000-0002-2579-8835; Email: danna@mit.edu

Authors

Catherine K. Badding − *Department of Chemistry, Massachusetts Institute of Technology, Cambridge, Massachusetts 02139, United States;* orcid.org/0000-0002-0448-5493

Eric A. Riesel − *Department of Chemistry, Massachusetts Institute of Technology, Cambridge, Massachusetts 02139, United States*

Ryan A. Murphy − *Department of Chemistry, Massachusetts Institute of Technology, Cambridge, Massachusetts 02139, United States*

Danilo Puggioni − *Department of Materials Science and Engineering, Northwestern University, Evanston, Illinois 60208, United States;* orcid.org/0000-0002-2128-4191

Dmitry Popov − *Advanced Photon Source, Argonne National Laboratory, Lemont, Illinois 60439, United States*

Gilberto Fabbris − *Advanced Photon Source, Argonne National Laboratory, Lemont, Illinois 60439, United States;* orcid.org/0000-0001-8278-4985

Daniel Haskel − *Advanced Photon Source, Argonne National Laboratory, Lemont, Illinois 60439, United States;* orcid.org/0000-0002-5532-5908

Complete contact information is available at: https://pubs.acs.org/10.1021/jacs.5c06874

Author Contributions

▽Authors C. K. Badding and E. A. Riesel contributed equally to this work.

Notes

The authors declare no competing financial interest.

■ ACKNOWLEDGMENTS

Authors D.E.F., A.B.A, C.K.B., E.A.R., and R.A.M. acknowledge the Department of Energy (DE-SC0023292) for support on all high-pressure synthesis and work creating and studying new permanent magnets. Portions of this work were performed at HPCAT (Sector 16) and Sector 4, Advanced Photon Source (APS), Argonne National Laboratory. HPCAT operations are supported by DOE-NNSA's Office of Experimental Sciences,

with partial instrumentation funding by NSF. The Advanced Photon Source is a U.S. Department of Energy (DOE) Office of Science User Facility operated for the DOE Office of Science by Argonne National Laboratory, under Contract No. DE-AC02-06CH11357. E.A.R. and C.K.B. acknowledge support from the National Science Foundation Graduate Research Fellowship, under Grant No. DGE-2141064). This work was carried out in part using MIT.nano's facilities. D.P. and J.M.R. were supported by the National Science Foundation (NSF), under Award No. DMR-2413680. They thank Max Hauschildt and Dawson Smith for early computational work on $MnBi_2$ supported by NSF through the Center for the Mechanical Control of Chemistry (No. CHE-2303044), part of the National Science Foundation (NSF) Centers for Chemical Innovation (CCI) program, Research Experience for Undergraduates (REU) program. We gratefully acknowledge Dr. Michael K. Wojnar for the insightful discussions and helpful comments on the manuscript. We thank Curtis Kenny-Benson for technical support setting up the resistive heating for our synthesis. C.K.B. and E.A.R. acknowledge support from the NSF-GRFP.

REFERENCES

(1) Gutfleisch, O.; Willard, M. A.; Brück, E.; Chen, C. H.; Sankar, S. G.; Liu, J. P. Magnetic Materials and Devices for the 21st Century: Stronger, Lighter, and More Energy Efficient. *Adv. Mater.* **2011**, *23* (7), 821−842.

(2) Jadhav, A. P.; Hussain, A.; Lee, J. H.; Baek, Y. K.; Choi, C. J.; Kang, Y. S. One Pot Synthesis of Hard Phase $Nd_2Fe_{14}B$ Nanoparticles and $Nd_2Fe_{14}B/\alpha$-Fe Nanocomposite Magnetic Materials. *New J. Chem.* **2012**, *36* (11), 2405−2411.

(3) Yakout, S. M. Spintronics: Future Technology for New Data Storage and Communication Devices. *J. Supercond Nov Magn* **2020**, *33* (9), 2557−2580.

(4) Bismanol: NOL Develops New Magnetic Material. *Phys. Today* **1952**, *5* (8), 19−20.

(5) Adams, E.; Hubbard, W. M.; Syeles, A. M. A New Permanent Magnet from Powdered Manganese Bismuthide. *J. Appl. Phys.* **1952**, *23* (11), 1207−1211.

(6) Yang, Y. B.; Chen, X. G.; Guo, S.; Yan, A. R.; Huang, Q. Z.; Wu, M. M.; Chen, D. F.; Yang, Y. C.; Yang, J. B. Temperature Dependences of Structure and Coercivity for Melt-Spun MnBi Compound. *J. Magn. Magn. Mater.* **2013**, *330*, 106−110.

(7) Roberts, B. W. Neutron Diffraction Study of the Structures and Magnetic Properties of Manganese Bismuthide. *Phys. Rev.* **1956**, *104* (3), 607−616.

(8) Heikes, R. R. Magnetic Transformation in MnBi. *Phys. Rev.* **1955**, *99* (2), 446−447.

(9) Gibson, Q. D.; Robertson, C. M.; Dyer, M. S.; Zanella, M.; Surta, T. W.; Daniels, L. M.; Claridge, J. B.; Alaria, J.; Rosseinsky, M. J. Single Crystal Growth and Properties of the Polar Ferromagnet $Mn_{1.05}Bi$ with Kagome Layers, Huge Magnetic Anisotropy and Slow Spin Dynamics. *Phys. Rev. Mater.* **2022**, *6* (11), 114405.

(10) Yang, J. B.; Yang, Y. B.; Chen, X. G.; Ma, X. B.; Han, J. Z.; Yang, Y. C.; Guo, S.; Yan, A. R.; Huang, Q. Z.; Wu, M. M.; Chen, D. F. Anisotropic Nanocrystalline MnBi with High Coercivity at High Temperature. *Appl. Phys. Lett.* **2011**, *99* (8), 082505.

(11) Yang, J. B.; Kamaraju, K.; Yelon, W. B.; James, W. J.; Cai, Q.; Bollero, A. Magnetic Properties of the MnBi Intermetallic Compound. *Appl. Phys. Lett.* **2001**, *79* (12), 1846−1848.

(12) McGuire, M. A.; Cao, H.; Chakoumakos, B. C.; Sales, B. C. Symmetry-Lowering Lattice Distortion at the Spin Reorientation in MnBi Single Crystals. *Phys. Rev. B* **2014**, *90* (17), 174425.

(13) Choi, Y.; Ryan, P. J.; McGuire, M. A.; Sales, B. C.; Kim, J.-W. Giant Magnetostriction Effect near Onset of Spin Reorientation in MnBi. *Appl. Phys. Lett.* **2018**, *112* (19), 192411.

(14) Guillaud, C. Polymorphisme du composé défini MnBi aux températures de disparition et de réapparition de l'aimantation spontanée. *J. Phys. Radium* **1951**, *12* (2), 143−143.

(15) Hihara, T.; Kōi, Y. Nuclear Magnetic Resonance Study of the Easy Axis of Magnetization in Manganese Bismuthide. *J. Phys. Soc. Jpn.* **1970**, *29* (2), 343−349.

(16) Andresen, A. F.; Halg, W.; Fischer, P.; Stoll, E.; Eriksson, G.; Blinc, R.; Pausak, S.; Ehrenberg, L.; Dumanovic, J. The Magnetic and Crystallographic Properties of MnBi Studied by Neutron Diffraction. *Acta Chem. Scand.* **1967**, *21* (6), 1543−1554.

(17) Choi, Y.; Jiang, X.; Bi, W.; Lapa, P.; Chouhan, R. K.; Paudyal, D.; Varga, T.; Popov, D.; Cui, J.; Haskel, D.; Jiang, J. S. Element-Resolved Magnetism across the Temperature- and Pressure-Induced Spin Reorientation in MnBi. *Phys. Rev. B* **2016**, *94* (18), 184433.

(18) Chen, T.; Stutius, W. The Phase Transformation and Physical Properties of the MnBi and $Mn_{1.08}Bi$ Compounds. *IEEE Trans. Magn.* **1974**, *10* (3), 581−586.

(19) Walsh, J. P. S.; Clarke, S. M.; Puggioni, D.; Tamerius, A. D.; Meng, Y.; Rondinelli, J. M.; Jacobsen, S. D.; Freedman, D. E. $MnBi_2$: A Metastable High-Pressure Phase in the Mn−Bi System. *Chem. Mater.* **2019**, *31* (9), 3083−3088.

(20) Park, J.; Hong, Y.-K.; Lee, J.; Lee, W.; Kim, S.-G.; Choi, C.-J. Electronic Structure and Maximum Energy Product of MnBi. *Metals* **2014**, *4* (3), 455−464.

(21) Torchio, R.; Kvashnin, Y. O.; Marini, C.; Mathon, O.; Garbarino, G.; Mezouar, M.; Wright, J. P.; Bruno, P.; Genovese, L.; Baudelet, F.; Meneghini, C.; Mobilio, S.; Morley, N. A.; Gibbs, M. R. J.; Pascarelli, S. Pressure-Induced Structural and Magnetic Phase Transitions in Ordered and Disordered Equiatomic FeCo. *Phys. Rev. B* **2013**, *88* (18), 184412.

(22) Hsieh, S.; Bhattacharyya, P.; Zu, C.; Mittiga, T.; Smart, T. J.; Machado, F.; Kobrin, B.; Höhn, T. O.; Rui, N. Z.; Kamrani, M.; Chatterjee, S.; Choi, S.; Zaletel, M.; Struzhkin, V. V.; Moore, J. E.; Levitas, V. I.; Jeanloz, R.; Yao, N. Y. Imaging Stress and Magnetism at High Pressures Using a Nanoscale Quantum Sensor. *Science* **2019**, *366* (6471), 1349−1354.

(23) Mathon, O.; Baudelet, F.; Itié, J. P.; Polian, A.; d'Astuto, M.; Chervin, J. C.; Pascarelli, S. Dynamics of the Magnetic and Structural α-ϵ Phase Transition in Iron. *Phys. Rev. Lett.* **2004**, *93* (25), 255503.

(24) Torchio, R.; Monza, A.; Baudelet, F.; Pascarelli, S.; Mathon, O.; Pugh, E.; Antonangeli, D.; Itié, J. P. Pressure-Induced Collapse of Ferromagnetism in Cobalt up to 120 GPa as Seen via x-Ray Magnetic Circular Dichroism. *Phys. Rev. B* **2011**, *84* (6), 060403.

(25) Torchio, R.; Kvashnin, Y. O.; Pascarelli, S.; Mathon, O.; Marini, C.; Genovese, L.; Bruno, P.; Garbarino, G.; Dewaele, A.; Occelli, F.; Loubeyre, P. X-Ray Magnetic Circular Dichroism Measurements in Ni up to 200 GPa: Resistant Ferromagnetism. *Phys. Rev. Lett.* **2011**, *107* (23), 237202.

(26) Maxwell, E. Mutual Inductance Bridge for Ac Susceptibility Measurements at Low Frequencies. *Rev. Sci. Instrum.* **1965**, *36* (4), 553−554.

(27) McKim, F. R.; Wolf, W. P. An Improved Inductance Method for Measuring Susceptibilities of Small Paramagnetic Specimens at Low Temperatures. *J. Sci. Instrum.* **1957**, *34* (2), 64.

(28) Hu, T.-L.; Wang, X.; Han, B.; Li, Y.; Huang, F.-X.; Zhou, Q.; Zhang, T. Magnetic Transition of Ferromagnetic Material at High Pressure Using a Novel System. *Chinese Physics B* **2013**, *22* (12), 120701.

(29) Jackson, D. D.; Aracne-Ruddle, C.; Malba, V.; Weir, S. T.; Catledge, S. A.; Vohra, Y. K. Magnetic Susceptibility Measurements at High Pressure Using Designer Diamond Anvils. *Rev. Sci. Instrum.* **2003**, *74* (4), 2467−2471.

(30) Wang, X.; Misek, M.; Jacobsen, M. K.; Kamenev, K. V. Use of an Advanced Composite Material in Construction of a High Pressure Cell for Magnetic Ac Susceptibility Measurements. *High Pressure Research* **2014**, *34* (4), 371−384.

(31) Timofeev, Y. A.; Struzhkin, V. V.; Hemley, R. J.; Mao, H.; Gregoryanz, E. A. Improved Techniques for Measurement of

https://doi.org/10.1021/jacs.5c06874
J. Am. Chem. Soc. 2025, 147, 25129−25135

Superconductivity in Diamond Anvil Cells by Magnetic Susceptibility. *Review of scientific instruments* **2002**, *73* (2), 371−377.
(32) Balédent, V.; Nataf, L.; Rueff, J.-P. Exceptionally Robust Magnetism and Structure of $SrFeO_2$ above 100 GPa. *Sci. Rep.* **2022**, *12* (1), 16018.
(33) Haskel, D.; Fabbris, G.; Kim, J. H.; Veiga, L. S. I.; Mardegan, J. R. L.; Escanhoela, C. A.; Chikara, S.; Struzhkin, V.; Senthil, T.; Kim, B. J.; Cao, G.; Kim, J.-W. Possible Quantum Paramagnetism in Compressed Sr_2IrO_4. *Phys. Rev. Lett.* **2020**, *124* (6), 067201.
(34) Ding, Y.; Haskel, D.; Ovchinnikov, S. G.; Tseng, Y.-C.; Orlov, Y. S.; Lang, J. C.; Mao, H. Novel Pressure-Induced Magnetic Transition in Magnetite (Fe_3O_4). *Phys. Rev. Lett.* **2008**, *100* (4), 045508.
(35) Haskel, D.; Tseng, Y. C.; Souza-Neto, N. M.; Lang, J. C.; Sinogeikin, S.; Mudryk, Ya; Gschneidner, K. A.; Pecharsky, V. K. Magnetic Spectroscopy at High Pressures Using X-Ray Magnetic Circular Dichroism. *High Press Res.* **2008**, *28* (3), 185−192.
(36) Baudelet, F.; Dubuisson, J. M.; Hébert, C.; Créoff, C.; Pointal, L.; Andouard, R.; Odin, S.; Dartyge, E.; Krill, G.; Giorgetti, C.; Chervin, J. C.; Itié, J. P.; Polian, A.; Fontaine, A.; Pizzini, S.; Kappler, J. P. Two Recent Developments in XMCD. *J. Synchrotron Rad* **1998**, *5* (3), 992−994.
(37) Feng, Y.; Jaramillo, R.; Srajer, G.; Lang, J. C.; Islam, Z.; Somayazulu, M. S.; Shpyrko, O. G.; Pluth, J. J.; Mao, H. -k.; Isaacs, E. D.; Aeppli, G.; Rosenbaum, T. F. Pressure-Tuned Spin and Charge Ordering in an Itinerant Antiferromagnet. *Phys. Rev. Lett.* **2007**, *99* (13), 137201.
(38) Duman, E.; Acet, M.; Wassermann, E. F.; Itié, J. P.; Baudelet, F.; Mathon, O.; Pascarelli, S. Magnetic Instabilities in Fe_3C Cementite Particles Observed with Fe *K*-Edge X-Ray Circular Dichroism under Pressure. *Phys. Rev. Lett.* **2005**, *94* (7), 075502.
(39) Ishimatsu, N.; Maruyama, H.; Kawamura, N.; Suzuki, M.; Ohishi, Y.; Ito, M.; Nasu, S.; Kawakami, T.; Shimomura, O. Pressure-Induced Magnetic Transition in Fe_4N Probed by Fe *K*-Edge XMCD Measurement. *J. Phys. Soc. Jpn.* **2003**, *72* (9), 2372−2376.
(40) Iota, V.; Klepeis, J.-H. P.; Yoo, C.-S.; Lang, J.; Haskel, D.; Srajer, G. Electronic Structure and Magnetism in Compressed 3*d* Transition Metals. *Appl. Phys. Lett.* **2007**, *90* (4), 042505.
(41) Haskel, D.; Tseng, Y. C.; Lang, J. C.; Sinogeikin, S. Instrument for X-Ray Magnetic Circular Dichroism Measurements at High Pressures. *Rev. Sci. Instrum.* **2007**, *78* (8), No. 083904.
(42) Haskel, D.; Fabbris, G.; Zhernenkov, M.; Kong, P. P.; Jin, C. Q.; Cao, G.; van Veenendaal, M. Pressure Tuning of the Spin-Orbit Coupled Ground State in Sr_2O_4. *Phys. Rev. Lett.* **2012**, *109* (2), No. 027204.
(43) Thole, B. T.; van der Laan, G.; Sawatzky, G. A. Strong Magnetic Dichroism Predicted in the $M_{4,5}$ X-Ray Absorption Spectra of Magnetic Rare-Earth Materials. *Phys. Rev. Lett.* **1985**, *55* (19), 2086−2088.
(44) van der Laan, G.; Thole, B. T.; Sawatzky, G. A.; Goedkoop, J. B.; Fuggle, J. C.; Esteva, J.-M.; Karnatak, R.; Remeika, J. P.; Dabkowska, H. A. Experimental Proof of Magnetic X-Ray Dichroism. *Phys. Rev. B* **1986**, *34* (9), 6529−6531.
(45) Schütz, G.; Wagner, W.; Wilhelm, W.; Kienle, P.; Zeller, R.; Frahm, R.; Materlik, G. Absorption of Circularly Polarized x Rays in Iron. *Phys. Rev. Lett.* **1987**, *58* (7), 737−740.
(46) Carra, P.; Altarelli, M. Dichroism in the X-Ray Absorption Spectra of Magnetically Ordered Systems. *Phys. Rev. Lett.* **1990**, *64* (11), 1286−1288.
(47) Stöhr, J. Exploring the Microscopic Origin of Magnetic Anisotropies with X-Ray Magnetic Circular Dichroism (XMCD) Spectroscopy. *J. Magn. Magn. Mater.* **1999**, *200* (1), 470−497.
(48) van der Laan, G.; Figueroa, A. I. X-Ray Magnetic Circular Dichroism—A Versatile Tool to Study Magnetism. *Coord. Chem. Rev.* **2014**, *277*−*278*, 95−129.
(49) Antropov, V. P.; Antonov, V. N.; Bekenov, L. V.; Kutepov, A.; Kotliar, G. Magnetic Anisotropic Effects and Electronic Correlations in MnBi Ferromagnet. *Phys. Rev. B* **2014**, *90* (5), No. 054404.
(50) Thole, B. T.; Carra, P.; Sette, F.; van der Laan, G. X-Ray Circular Dichroism as a Probe of Orbital Magnetization. *Phys. Rev. Lett.* **1992**, *68* (12), 1943−1946.
(51) Carra, P.; Thole, B. T.; Altarelli, M.; Wang, X. X-Ray Circular Dichroism and Local Magnetic Fields. *Phys. Rev. Lett.* **1993**, *70* (5), 694−697.
(52) Kim, D. H.; Lee, E.; Kim, H. W.; Seong, S.; Yang, S.-M.; Park, H.-S.; Hong, J.; Kim, Y.; Kim, J.-Y.; Kang, J.-S. Angle-Dependent X-Ray Magnetic Circular Dichroism Study of Enhanced Perpendicular Magnetic Anisotropy in Hybrid $[CoO/Pd]_2[Co/Pd]_7$ Multilayers. *J. Magn. Magn. Mater.* **2017**, *432*, 450−454.
(53) Nakajima, N.; Koide, T.; Shidara, T.; Miyauchi, H.; Fukutani, H.; Fujimori, A.; Iio, K.; Katayama, T.; Nývlt, M.; Suzuki, Y. Perpendicular Magnetic Anisotropy Caused by Interfacial Hybridization via Enhanced Orbital Moment in Co/Pt Multilayers: Magnetic Circular X-Ray Dichroism Study. *Phys. Rev. Lett.* **1998**, *81* (23), 5229−5232.
(54) Bruno, P. Tight-Binding Approach to the Orbital Magnetic Moment and Magnetocrystalline Anisotropy of Transition-Metal Monolayers. *Phys. Rev. B* **1989**, *39* (1), 865−868.
(55) Soares, M. M.; Lamirand, A. D.; Ramos, A. Y.; De Santis, M.; Tolentino, H. C. N. Orbital Moment Anisotropy in Ultrathin FePt Layers. *Phys. Rev. B* **2014**, *90* (21), 214403.
(56) Coehoorn, R.; de Groot, R. A. The Electronic Structure of MnBi. *J. Phys. F: Met. Phys.* **1985**, *15* (10), 2135.
(57) Ravindran, P.; Delin, A.; James, P.; Johansson, B.; Wills, J. M.; Ahuja, R.; Eriksson, O. Magnetic, Optical, and Magneto-Optical Properties of MnX (X = As, Sb, or Bi) from Full-Potential Calculations. *Phys. Rev. B* **1999**, *59* (24), 15680−15693.
(58) Ko, K.-T.; Kim, K.; Kim, S. B.; Kim, H.-D.; Kim, J.-Y.; Min, B. I.; Park, J.-H.; Chang, F.-H.; Lin, H.-J.; Tanaka, A.; Cheong, S.-W. RKKY Ferromagnetism with Ising-Like Spin States in Intercalated $Fe_{1/4}TaS_2$. *Phys. Rev. Lett.* **2011**, *107* (24), 247201.
(59) Bland, J. A. C.; Heinrich, B. Magnetic Anisotropy, Magnetization and Band Structure. *Ultrathin Magnetic Structures I: An Introduction to the Electronic, Magnetic and Structural Properties* **1994**, 21−90.
(60) Teh, W. H.; Chaudhary, V.; Chen, S.; Lim, S. H.; Wei, F.; Lee, J. Y.; Wang, P.; Padhy, S. P.; Tan, C. C.; Ramanujan, R. V. High Throughput Multi-Property Evaluation of Additively Manufactured Co-Fe-Ni Materials Libraries. *Additive Manufacturing* **2022**, *58*, 102983.
(61) Nordström, L.; Johansson, B.; Brooks, M. S. S. Calculated Magnetic Moments of $Nd_2Fe_{14}B$. *J. Appl. Phys.* **1991**, *69* (8), 5708−5710.
(62) Yehia, S.; Aly, S.; Hamid, A. S.; Aly, A. E.; Hammam, M. Magnetic Properties and Band Structure Calculation of $SmCo_5$. *Int. J. Pure Appl. Phys.* **2006**, *2* (3), 205−213.
(63) Landa, A.; Lordi, V.; Soderlind, P.; Turchi, P. E. *$SmCo_5$-Based Compounds Doped with Fe and Ni for High-Performance Permanent Magnets;* US 2020/0318222 A1, 2020.

https://doi.org/10.1021/jacs.5c06874
J. Am. Chem. Soc. 2025, 147, 25129−25135